

# Imaging of granular sources in high energy heavy ion collisions

Zhi-Tao Yang<sup>1</sup>, Wei-Ning Zhang<sup>1,2\*</sup>, Lei Huo<sup>1</sup>, and Jing-Bo Zhang<sup>1</sup>

<sup>1</sup>*Department of Physics, Harbin Institute of Technology,*

*Harbin, Heilongjiang 150006, China*

<sup>2</sup>*School of Physics and Optoelectronic Technology,*

*Dalian University of Technology, Dalian, Liaoning 116024, China*

(Dated: January 10, 2019)

## Abstract

We investigate the source imaging for a granular pion-emitting source model in high energy heavy ion collisions. The two-pion source functions of the granular sources exhibit a two-tiered structure. Using a parametrized formula of granular two-pion source function, we examine the two-tiered structure of the source functions for the imaging data of Au+Au collisions at Alternating Gradient Synchrotron (AGS) and Relativistic Heavy Ion Collider (RHIC). We find that the imaging technique introduced by Brown and Danielewicz is suitable for probing the granular structure of the sources. Our data-fitting results indicate that there is not visible granularity for the sources at AGS energies. However, the data for the RHIC collisions with the selections of  $40 < \text{centrality} < 90\%$  and  $0.20 < k_T < 0.36 \text{ GeV}/c$  are better described by the model with granular emission than that of one Gaussian. The model with granular source has more parameters than the simple Gaussian, hence can describe more complicated shapes.

PACS numbers: 25.75.-q, 25.75.Nq, 25.75.Gz

---

\* wnzhang@dlut.edu.cn

## I. INTRODUCTION

Two-pion Hanbury-Brown-Twiss (HBT) interferometry is a powerful tool of detection of the space-time structure of particle-emitting sources produced in high energy heavy ion collisions [1, 2, 3, 4]. In conventional two-pion HBT analysis one needs fitting the two-pion HBT correlation functions with parametrized formulas to obtain quantitatively the source space-time results. So the explanations of the HBT results are model depended. Imaging technique introduced by Brown and Danielewicz [5, 6, 7] is a model-independent way. It can be used to extract the source geometry pictures (source function) directly from the two-pion correlation functions. This technique has been developed and used in high energy heavy ion collisions [8, 9, 10, 11, 12, 13, 14, 15, 16, 17, 18, 19, 20].

Recently, there has been much progress in understanding of the process of nucleus-nucleus collisions at RHIC. However, there are still many unsolved problems. One of them is the so-called HBT puzzle,  $R_{\text{out}}/R_{\text{side}} \approx 1$  [21, 22, 23, 24]. Here  $R_{\text{out}}$  and  $R_{\text{side}}$  are the transverse HBT radii parallel and perpendicular to the pion pair momentum [25, 26]. In Ref. [27] a granular source model of quark-gluon plasma (QGP) droplets was put forth to explain the HBT puzzle. The suggestion was based on the observation that in the hydrodynamic calculations for the granular source the average particle emission time scales with the initial radius of the droplet, whereas the spacial size of the source is the scale of the distribution of the droplets. For a granular source with many of the small droplets distributed in a relatively large region, the HBT radius  $R_{\text{out}}$  can be close to  $R_{\text{side}}$  [27]. In Ref. [28] the authors further investigated the elliptic flow and HBT radii as a function of pion transverse momentum for an improved granular source model of QGP droplets. They argued that although a granular structure was suggested earlier as the signature of a first-order phase transition [27, 29, 30, 31, 32, 33, 34, 35, 36, 37], the occurrence of granular structure may not be limited to first-order phase transition [28, 38]. The large fluctuations of initial matter distribution [39, 40, 41, 42] in high energy heavy ion collisions may facilitate the occurrence of instability of the system during its subsequent expansion and fragmentation to many granular droplets together with surface tension effect [28, 38].

Recent researches on event-by-event two-pion Bose-Einstein correlations in smoothed particle hydrodynamics indicate that the particle-emitting sources produced at RHIC energy are inhomogeneous and there is a granular structure of many “lumps” (droplets) [43].

For a simple granular source model we will show that the two-pion source function has a two-tiered structure. In small relative coordinate  $r$  region, the source function exhibits an enhancement because of the higher density in the droplets. Previous RHIC experimental imaging researches are mainly focused on the long-range tail of the source functions at large  $r$  [17, 18, 19, 20], and the deviations of the source function from Gaussian distribution in the large  $r$  region are believed mainly the contribution of long-lived resonances [17, 44]. In this paper we will focus our attention on the source functions in small  $r$  region. We will investigate the imaging of granular sources. We will examine the two-tiered structure of the source functions for the AGS and RHIC imaging data of Au+Au [10, 17]. Our results indicate that the imaging technique is suitable for probing the granular structure of the particle-emitting sources. There is not visible granularity for the sources in Au+Au collisions at AGS energies. However, the data for the RHIC collisions with the selections of  $40 < \text{centrality} < 90\%$  and  $0.20 < k_T < 0.36$  GeV/c are better described by the model with granular emission than from that of one Gaussian.

## II. IMAGING TECHNIQUE

For the convenience of discussion later in the paper, we start out with a brief review of the imaging technique of Brown and Danielewicz [5, 6, 7].

Based on the Koonin-Pratt formulism [45, 46], the two-pion HBT correlation function may be expressed in the center-of-mass frame of the particle pair as [7, 9, 10, 15]:

$$C(\mathbf{q}) - 1 = \int d\mathbf{r} K(\mathbf{q}, \mathbf{r}) S(\mathbf{r}), \quad (1)$$

where  $\mathbf{q} = \mathbf{p}_1 - \mathbf{p}_2$  is the relative momentum of the pion pair,  $\mathbf{r}$  is the relative separation of emission points of the two particles,  $K(\mathbf{q}, \mathbf{r}) = |\Phi_{\mathbf{q}}(\mathbf{r})|^2 - 1$ , where  $\Phi_{\mathbf{q}}(\mathbf{r})$  is the relative wave function of the pair. Neglecting the final-state interaction of the pion pair, one has

$$\Phi_{\mathbf{q}}(\mathbf{r}) = \frac{1}{\sqrt{2}}(e^{i\mathbf{q}\cdot\mathbf{r}/2} + e^{-i\mathbf{q}\cdot\mathbf{r}/2}). \quad (2)$$

In Eq. (1),  $S(\mathbf{r})$  is the so-called two-particle source function. It may be written with Wigner function as [7, 9],

$$S(\mathbf{r}) = \int dt \int d^3R dT D(\mathbf{R} + \mathbf{r}/2, T + t/2, \mathbf{p}_1) \times D(\mathbf{R} - \mathbf{r}/2, T - t/2, \mathbf{p}_2). \quad (3)$$

Here the Wigner functions are normalized particle emission rates,

$$D(\mathbf{r}, t, \mathbf{p}) = \frac{E d^7 N}{d^3 r dt d^3 p} \bigg/ \int \frac{E d^3 N}{d^3 p} d^3 p. \quad (4)$$

For a spherically symmetric source function,  $S(\mathbf{r}) = S(r)$ , performing the angle integrations on the right hand of Eq. (1), one gets the angle-averaged version of Eq. (1) as,

$$\mathcal{R}(q_{\text{inv}}) \equiv C(q_{\text{inv}}) - 1 = 4\pi \int dr r^2 K(q_{\text{inv}}, r) S(r). \quad (5)$$

Here  $q_{\text{inv}} = \sqrt{\mathbf{q}^2 - q_0^2}$ ,

$$K(q_{\text{inv}}, r) = \sin(q_{\text{inv}} r) / (q_{\text{inv}} r). \quad (6)$$

Equation (5) now is suitable in any frame and the problem of imaging becomes inverting  $K(q_{\text{inv}}, r)$  with measured correlation function  $\mathcal{R}(q_{\text{inv}})$ . After expanding the source function  $S(r)$  in  $b$ -spline basis [7],

$$S(r) = \sum_j S_j B_j(r), \quad (7)$$

the inversion problem reduces to the problem of solving the matrix equation

$$\mathcal{R}(q_i) = \sum_j K_{ij} S_j, \quad (8)$$

where  $\mathcal{R}(q_i)$  denotes the value of the correlation function at the  $i$ th bin of  $q_{\text{inv}}$ , and

$$K_{ij} = \frac{4\pi}{\Delta q} \int_{q_i - \Delta q/2}^{q_i + \Delta q/2} dq_{\text{inv}} \int_0^\infty dr r^2 K(q_{\text{inv}}, r) B_j(r), \quad (9)$$

where  $\Delta q$  is the bin size of  $q_{\text{inv}}$ .

In present paper, the minimization package MINUIT [47] was used to minimize the  $\chi^2$  between the measured and calculated correlation functions.

### III. SOURCE FUNCTION IMAGING FOR STATIC GRANULAR SOURCES

In this section we examine the source function imaging for static granular sources. Although static source is not a realistic case, its source function may still be used as a parametrized formula in the analysis for evolving sources.

For the granular source model, particles are emitted from dispersed droplets [27, 28, 30, 34, 35, 36, 37]. Assuming that the granular source has the same  $N$  droplets and the

distribution of the particle emission points in a droplet has Gaussian form, the normalized source density distribution is given by [36]

$$D(\mathbf{x}) = \frac{1}{N(\sqrt{2\pi}a)^3} \sum_{i=1}^N \exp \left[ -\frac{(\mathbf{x} - \mathbf{X}_i)^2}{2a^2} \right], \quad (10)$$

where  $a$  is the “radius” of the droplets and  $\mathbf{X}_i$  is the spatial coordinate of the  $i$ th droplet center. Inserting this distribution into Eq. (3), we obtain

$$\begin{aligned} S(\mathbf{r}) &= \frac{1}{N^2(\sqrt{4\pi}a)^3} \sum_{i,j=1}^N \exp \left[ -\frac{(\mathbf{r} - \mathbf{X}_{ij})^2}{4a^2} \right] \\ &= \frac{1}{N^2(\sqrt{4\pi}a)^3} \exp \left( -\frac{r^2}{4a^2} \right) \\ &\quad \times \sum_{i,j=1}^N \exp \left( -\frac{|\mathbf{X}_{ij}|^2}{4a^2} \right) \exp \left( \frac{r|\mathbf{X}_{ij}| \cos \alpha}{2a^2} \right), \end{aligned} \quad (11)$$

where  $\mathbf{X}_{ij} = \mathbf{X}_i - \mathbf{X}_j$ ,  $\alpha$  is the angle between  $\mathbf{r}$  and  $\mathbf{X}_{ij}$ . The source function presents fluctuation due to the factor  $\exp \left( \frac{r|\mathbf{X}_{ij}| \cos \alpha}{2a^2} \right)$ .

Due to limited number of produced particles per event, conventional two-pion HBT interferometry analyses are based on averages over events. The correlation functions are obtained from the correlated pion pairs (the two identical pions in each of the pairs are from the same event) of all sample events. Accordingly, the source function for the mixed-events of the granular source,  $S^{\text{Gran}}(r)$ , should be the average of Eq. (11) over all the events. Assuming that the droplet centers in the granular source obey the Gaussian distribution,  $P(\mathbf{X}_i) \sim \exp(-\mathbf{X}_i^2/2R_{\text{gr}}^2)$ , we get

$$\begin{aligned} S^{\text{Granu}}(r) &= \frac{1}{N} \frac{1}{(\sqrt{4\pi}a)^3} \exp \left( -\frac{r^2}{4a^2} \right) + \left( 1 - \frac{1}{N} \right) \\ &\quad \times \frac{1}{(\sqrt{4\pi}\sqrt{a^2 + R_{\text{gr}}^2})^3} \exp \left[ -\frac{r^2}{4(a^2 + R_{\text{gr}}^2)} \right]. \end{aligned} \quad (12)$$

Compared with the two-particle source function of the Gaussian source model usually used [7, 10, 15],

$$S^{\text{Gauss}}(r) = \frac{1}{(\sqrt{4\pi}R_{\text{ga}})^3} \exp \left( -\frac{r^2}{4R_{\text{ga}}^2} \right), \quad (13)$$

the source function of the granular source consists of two exponential terms, which correspond to that the two particles from the same droplet and from different droplets respectively. This “two-tiered structure” of the source function is consistent with the two-tiered

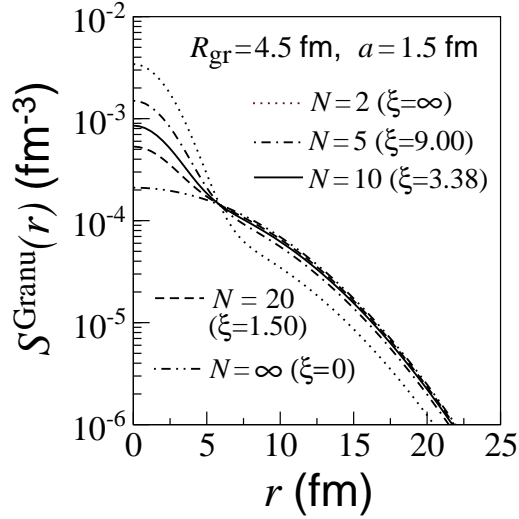


FIG. 1: The two-particle source functions of granular sources.

structure of the correlation function for the granular source [30, 34]. It is most apparent when  $N = 2$ , and disappears when  $N \rightarrow \infty$ . For  $R_{\text{gr}}^2 \gg a^2$ , the coefficient ratio of the two terms in Eq. (12) is  $(R_{\text{gr}}/a)^3/(N-1)$ , which is a characteristic quantity for the two-tiered structure. Considering also  $N \geq 2$  for the granular source model, we introduce the quantity,

$$\xi = \frac{(R_{\text{gr}}/a)^3}{N-2}, \quad (14)$$

to characterize the granularity of the sources. For granular sources the values of  $\xi$  are between  $(0, \infty)$ , and a source will have not granularity when  $\xi \leq 0$ . In Fig. 1 we show the curves of  $S^{\text{Granu}}(r)$  as a function of the droplet number  $N$  for the granular sources with  $R_{\text{gr}} = 4.5$  fm and  $a = 1.5$  fm. One can see that the two-tiered structure is obvious for finite droplet numbers of the granular sources.

We next examine the imaging of the static granular source. In Fig. 2(a) we show the two-pion correlation function (CF) obtained from  $2 \times 10^5$  simulated two-pion events for the granular source with  $R_{\text{gr}} = 4.5$  fm and  $a = 1.5$  fm. For comparison, the correlation function for a Gaussian source with  $R_{\text{ga}} = 4.5$  fm is presented in Fig. 2(b). In the simulations, pions are emitted thermally from the sources at freeze-out temperature  $T_f = 150$  MeV. Figure 2(a') and (b') show the two-pion source functions (circle symbols) extracted from the two-pion correlation functions by the imaging technique. The curves in Fig. 2(a') and (b') are the results of the source function fit (SFF) with the formulas  $\lambda S^{\text{Granu}}(r)$  and  $\lambda S^{\text{Gauss}}(r)$ . Here  $\lambda$  is the parameter of source coherent factor in HBT interferometry [1, 2, 3, 4] and

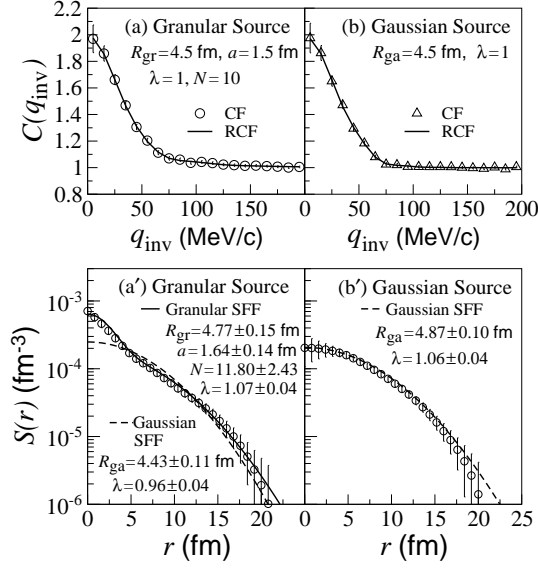


FIG. 2: (a, b) The two-pion correlation functions for granular and Gaussian sources. (a', b') The two-pion source functions extracted by imaging technique for the granular and Gaussian sources.

$S^{\text{Granu}}(r)$  and  $S^{\text{Gauss}}(r)$  are given by Eqs. (12) and (13), respectively. The corresponding fitting results are also presented in the figure. For the granular source the  $\chi^2/\text{NDF}$  for the granular SFF is 0.22, which is much smaller than that of 3.88 for the Gaussian SFF. The curves in Fig. 2(a) and (b) are the restored correlation functions (RCF) calculated by Eq. (5). From Fig. 2 one can see that although the two-pion correlation functions for the granular and Gaussian sources are almost the same in shape, the granular source function exhibits a clear enhancement in small  $r$  region, which reflects the higher source density in a droplet. So imaging technique is suitable for probing the granular structure of the sources.

Figure 3(a), (b), (c), and (d) show further the source functions for the granular sources with various source parameters. It can be seen that the two-tiered structure is more obvious for smaller droplet number  $N$  and smaller droplet radius  $a$ . One can still observe the two-tiered structure even  $\xi \approx 2$ .

#### IV. TWO-TIERED STRUCTURE OF SOURCE FUNCTIONS FOR EVOLVING SOURCES

In this section we investigate the two-tiered structure of the source functions for evolving sources. First we consider a simple granular source model of  $N$  evolving QGP droplets. We

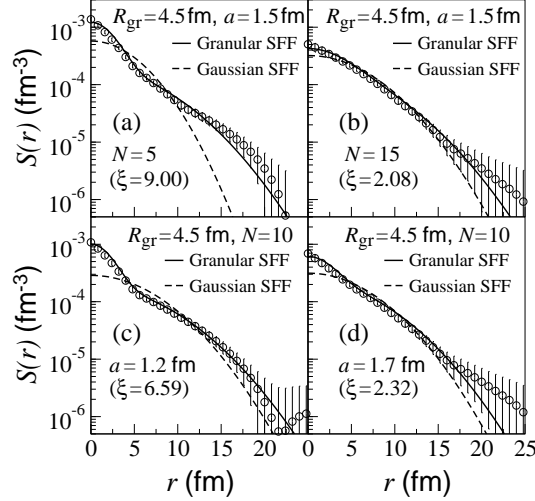


FIG. 3: The source functions for the granular sources with various parameters.

assume that all of the droplets in the source have the same initial conditions and evolve hydrodynamically in the same way [27, 37]. An equation of state of the entropy density suggested by QCD lattice gauge results [48, 49, 50] with the transition temperature  $T_c = 165$  MeV and the temperature width of the transition  $\Delta T = 0.05 T_c$  is used in the hydrodynamical calculations [27, 28, 37]. In our calculations the initial energy density of the droplets is taken to be  $\epsilon_0 = 3.75 T_c s_c$ , which is about two times of the density of quark matter at  $T_c$  [28, 50]. The initial distribution of the droplet centers is given by a Gaussian distribution with standard deviation  $R_0$ . For the case with an additional collective radial expansion, the droplet centers are assumed to have a constant radial velocity  $v_d$  in the center-of-mass frame of the granular source [27, 37]. The source freeze-out temperature is taken to be  $T_f = 150$  MeV.

Figure 4(a) and (b) show the source functions  $S(r)$  (circle symbols) obtained by the imaging technique from the two-pion correlation functions  $C(q_{\text{inv}})$  for the granular sources with the parameters  $R_0 = 5.0$  fm,  $v_d = 0.5$ , and  $\lambda = 1$ . The droplet number and initial droplet radius for the granular source of Fig. 4(a) are 5 and 2.5 fm, and they are 15 and 1.5 fm for the granular source of Fig. 4(b). One can see that the source functions of the granular sources have enhancements in small  $r$  region. With the granular SFF results one gets that the values of  $\xi$  for the two granular sources are  $4.85 \pm 2.94$  and  $4.66 \pm 2.83$ , respectively. The large  $\xi$  values indicate large granularity for the sources, which is consistent with the observations.



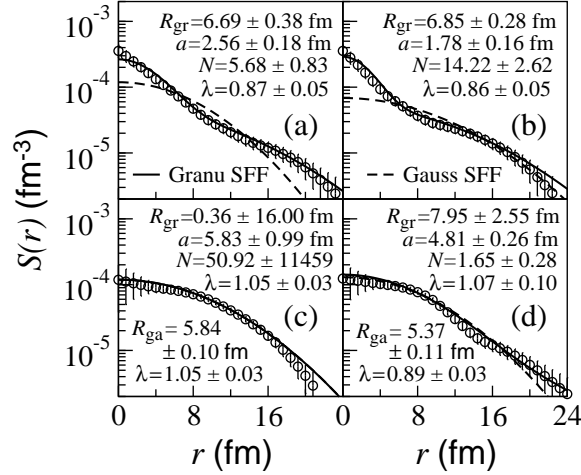


FIG. 4: The source functions for the evolving granular sources [(a) and (b)] and the expanding Gaussian sources [(c) and (d)].

For comparison, in Fig. 4(c) and (d) we show the source functions obtained by the imaging technique from the two-pion correlation functions for the sources with Gaussian distribution and additional radial expanding velocities 0.3 and 0.6, respectively. The standard deviation for the Gaussian distribution is taken to be 5.0 fm. From Fig. 4(c) it can be seen that for the Gaussian distribution source with smaller expanding velocity the granular and Gaussian SFF curves are almost overlapped. The granular SFF gives a very large  $N$ . For a large  $N$  one can see that the first term of the fitting formula Eq. (12) approaches zero and the two-tiered structure disappears. One can also see from Eq. (12) that in this case the fitting formula is almost independent of  $N$  and the parameters  $R_{\text{gr}}$  and  $a$  can be reduced to one parameter  $\sqrt{R_{\text{gr}}^2 + a^2}$  as  $R_{\text{ga}}$  in Eq. (13). So the fit is insensitive to the parameters  $N$  and  $R_{\text{gr}}$ . From Fig. 4(d) one can see that in small  $r$  region the two SFF curves are almost overlapped and there is only a small difference between the two SFF curves in large  $r$  region. We find that the granular SFF result of  $N$  is less than 2. In this case the source has not granularity. With the granular SFF results for the two expanding Gaussian sources we get that the values of the characteristic quantity of granularity  $\xi$  are  $4.813 \times 10^{-6} \pm 0.002$  and  $-12.900 \pm 4.185$ . They indicate that there is not granularity for the sources.

We next examine the two-tiered structure of the two-pion source functions for the imaging data in the Au+Au collisions at AGS [10] and RHIC [17]. The circle symbols in Fig. 5(a), (b), (c), and (d) show the two-pion source functions for 2, 4, 6, and 8 AGeV Au+Au

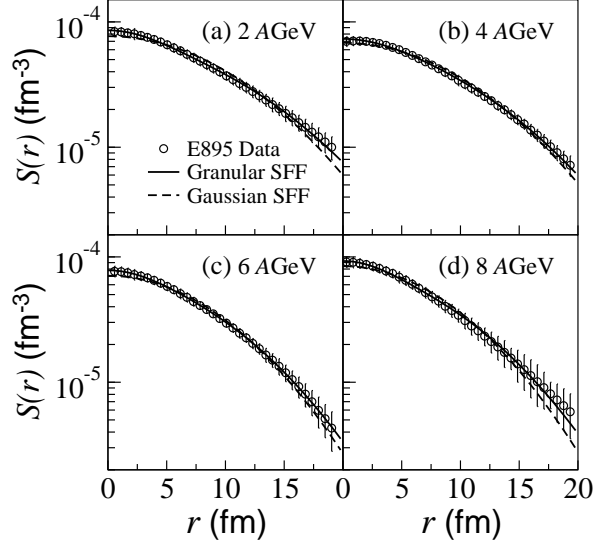


FIG. 5: The two-pion source functions ( $\circ$  symbols) for 2, 4, 6, and 8 AGeV Au+Au collisions [10] and the SFF curves.

collisions, respectively [10]. The circle symbols in Fig. 6(a) and (b) show the source functions for  $\sqrt{s_{NN}} = 200$  GeV Au+Au collisions with different cut conditions of centrality and average transverse momentum  $k_T$  of the pion pair. In Figs. 5 and 6, the solid and dashed curves are our granular and Gaussian SFF curves. The fitting results are listed in Table I. It can be seen that the  $\chi^2/\text{NDF}$  for the granular SFF are very small. This indicates that the data errors are large for the granular SFF and the granular SFF may distinguish more complicated source shapes if there is enough statistics. From Fig. 5 one cannot observe the two-tiered structure of the source functions in small  $r$  region. When we use the granular parametrized formula  $\lambda S^{\text{Granu}}(r)$  to fit the source functions we find that the errors of  $N$  are the same order of the values of  $N$ . In Table I we present the fit results for fixed  $N = 50$ . One can see that the values of  $\xi$  in Table I for the collisions at AGS energies are very small. So there is not visible granularity for the sources.

From Fig. 6 it can be seen that for the higher  $k_T$  most central collisions (a) the source function has not obvious two-tiered structure and the spheroidal (dot-line) [17], granular, and Gaussian SFF curves in small  $r$  region are almost overlapped. It indicates that there is not visible granularity for the source. However, for the lower  $k_T$  peripheral collisions (b) one can find an obvious two-tiered structure of the source function. In small  $r$  region the source function has an enhancement relative to the Gaussian SFF curve [see the insert in

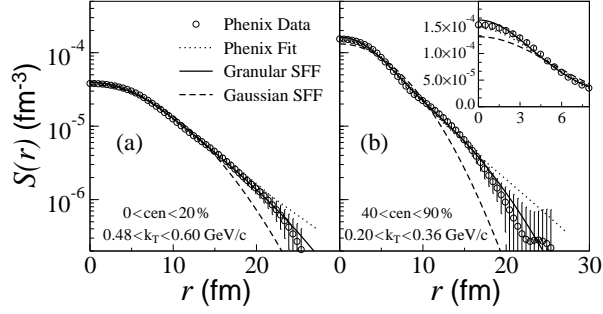


FIG. 6: The two-pion source functions ( $\circ$  symbols) for  $\sqrt{s_{NN}} = 200$  GeV Au+Au collisions [17] and the SFF curves.

TABLE I: The results of granular and Gaussian source function fits (SFF).

		AGS(a)	AGS(b)	AGS(c)	AGS(d)	RHIC(a)	RHIC(b)
Granular	$R_{gr}(\text{fm})$	$6.31 \pm 0.23$	$5.92 \pm 0.18$	$5.28 \pm 0.19$	$5.39 \pm 0.23$	$5.23 \pm 0.21$	$4.53 \pm 0.10$
SFF	$a(\text{fm})$	$2.67 \pm 0.16$	$2.92 \pm 0.18$	$2.51 \pm 0.21$	$2.35 \pm 0.17$	$3.90 \pm 0.13$	$2.56 \pm 0.05$
	$\lambda$	$0.93 \pm 0.05$	$0.77 \pm 0.02$	$0.57 \pm 0.02$	$0.65 \pm 0.04$	$0.24 \pm 0.01$	$0.39 \pm 0.01$
	$N$	50(fixed)	50(fixed)	50(fixed)	50(fixed)	$3.54 \pm 0.61$	$4.61 \pm 0.35$
	$\chi^2/\text{NDF}$	0.04	0.05	0.01	0.06	0.35	0.71
	$\xi$	$0.28 \pm 0.08$	$0.17 \pm 0.05$	$0.19 \pm 0.07$	$0.25 \pm 0.09$	$1.56 \pm 0.97$	$2.12 \pm 0.55$
Gaussian	$R_{ga}(\text{fm})$	$6.26 \pm 0.11$	$6.22 \pm 0.07$	$5.53 \pm 0.09$	$5.41 \pm 0.12$	$5.05 \pm 0.13$	$3.79 \pm 0.03$
SFF	$\lambda$	$0.84 \pm 0.03$	$0.73 \pm 0.02$	$0.53 \pm 0.02$	$0.59 \pm 0.03$	$0.21 \pm 0.01$	$0.32 \pm 0.01$
	$\chi^2/\text{NDF}$	0.62	0.46	0.32	0.41	3.72	10.87

Fig. 6(b)]. Based on the granular source explanation, the enhancement in small  $r$  region indicates that there are small droplets with higher density in the particle-emitting source. In Table I, the value of  $\xi$  for the case (b) is larger than that for the case (a), which is consistent with the observations. Further investigation for the reasons of the enhancement of source function in small  $r$  region will be of great interest.

## V. SUMMARY AND CONCLUSION

We investigated the source imaging for a granular pion-emitting source model. The two-pion source functions of the granular sources exhibit a two-tiered structure, which can be characterized by the quantity  $\xi = (R_{\text{gr}}/a)^3/(N-2)$ . In small relative coordinate  $r$  region, the granular two-pion source functions have an enhancement because of the higher density in the droplets. We find that the imaging technique is suitable for probing the granularity of the pion-emitting sources. Using a parametrized formula of granular source function, we examine the two-tiered structure of the source functions for the imaging data of Au+Au collisions at 2, 4, 6, 8 AGeV [10] and  $\sqrt{s_{NN}} = 200$  GeV [17]. Our analysis results indicate that there is not visible granularity for the sources produced in the collisions at the AGS energies and at RHIC energy with the selections  $0 < \text{centrality} < 20\%$  and  $0.48 < k_T < 0.60$  GeV/c. However, the data for the RHIC collisions with the selections  $40 < \text{centrality} < 90\%$  and  $0.20 < k_T < 0.36$  GeV/c are better described by the model with granular emission than from that of one Gaussian. The model with granular source has more parameters than the simple gaussian, hence can describe more complicated shapes.

Although our granular parametrized formula of source function is obtained from a static granular source model and does not include the effect of droplet overlap, the fitting results with the formula for evolving sources have still referential meaning. In this paper we only examine one-dimension imaging of granular sources. Because the longitudinal dynamics at the RHIC energy is very different from that at AGS energies, the examinations of the source imaging in different directions [13, 15, 16, 44] and at intermediate energies (*i. e.* SPS energies) will be of great interest. Further investigations on the source granularity and its variation with the centrality and particle transverse momentum in collisions will be also interesting issues.

### Acknowledgments

The authors would like to thank Dr. D. A. Brown for helpful discussions. This research was supported by the National Natural Science Foundation of China under Contracts No.

- [1] C. Y. Wong, *Introduction to High-Energy Heavy-Ion Collisions* (World Scientific, Singapore, 1994), Chap. 17.
- [2] U. A. Wiedemann and U. Heinz, Phys. Rept. **319**, 145 (1999).
- [3] R. M. Weiner, Phys. Rept. **327**, 249 (2000).
- [4] M. A. Lisa, S. Pratt, R. Soltz, U. Wiedemann, Ann. Rev. Nucl. Part. Sci. **55**, 357 (2005); nucl-ex/0505014.
- [5] D. A. Brown and P. Danielewicz, Phys. Lett. B **389**, 252 (1997).
- [6] D. A. Brown and P. Danielewicz, Phys. Rev. C **57**, 2474 (1998).
- [7] D. A. Brown and P. Danielewicz, Phys. Rev. C **64**, 014902 (2001).
- [8] S. Y. Panitkin and D. A. Brown, Phys. Rev. C **61**, 021901 (1999).
- [9] D. A. Brown, S. Y. Panitkin, and G. F. Bertsch, Phys. Rev. C **62**, 014904 (2000).
- [10] S. Y. Panitkin et al. (E895 Collaboration), Phys. Rev. Lett. **87**, 112304 (2001).
- [11] G. Verde, D. A. Brown, P. Danielewicz, C. K. Gelbke, W. G. Lynch, and M. B. Tsang, Phys. Rev. C **65**, 054609 (2002).
- [12] P. Chung et al. (E895 Collaboration), Phys. Rev. Lett. **91**, 162301 (2003).
- [13] P. Danielewicz, D. A. Brown, M. Heffner, S. Pratt, and R. Soltz, Acta Phys. Hung. A **22**, 253 (2005) [nucl-th/0407022].
- [14] P. Chung, A. Taranenko, R. Lacey, W. Holzmann, J. Alexander, M. Issah, Nucl. Phys. **A749**, 275c (2005).
- [15] D. A. Brown, A. Enokizono, M. Heffner, R. Soltz, P. Danielewicz, and S. Pratt, Phys. Rev. C **72**, 054902 (2005).
- [16] P. Danielewicz, and S. Pratt, Phys. Rev. C **75**, 034907 (2007).
- [17] S. S. Adler et al. (PHE Collaboration), Phys. Rev. Lett. **98**, 132301 (2007).
- [18] R. A. Lacy, nucl-ex/0701026.
- [19] S. Afanasiev *et al.* (PHENIX Collaboration), arXiv:0712.4372 [nucl-ex].
- [20] R. A. Lacy for the PHENIX Collaboration, arXiv:0805.1352 [nucl-ex].
- [21] C. Adler *et al.* (STAR Collaboration), Phys. Rev. Lett. **87**, 082301 (2001).
- [22] K. Adcox *et al.* (PHENIX Collaboration), Phys. Rev. Lett. **88**, 192302 (2002).

- [23] S. S. Adler *et al.* (PHENIX Collaboration), Phys. Rev. Lett. **93**, 152302 (2004).
- [24] J. Adams *et al.* (STAR Collaboration), Phys. Rev. C **71**, 044906 (2005).
- [25] S. Pratt, Phys. Rev. D **33**, 72 (1986); S. Pratt, T. Csörgo, and J. Zimányi, Phys. Rev. C **42**, 2646 (1990).
- [26] G. Bertsch, M. Gong, and M. Tohyama, Phys. Rev. C **37**, 1896 (1988); G. Bertsch, Nucl. Phys. A **498**, 173c (1989).
- [27] W. N. Zhang, M. J. Efaaf, and C. Y. Wong, Phys. Rev. C **70**, 024903 (2004).
- [28] W. N. Zhang, Y. Y. Ren, and C. Y. Wong, Phys. Rev. C **74**, 024908 (2006).
- [29] E. Witten, Phys. Rev. D **30**, 272 (1984).
- [30] S. Pratt, P. J. Siemens, and A. P. Vischer, Phys. Rev. Lett **68**, 1109 (1992).
- [31] L. P. Csernai and J. I. Kapusta, Phys. Rev. D **46**, 1379 (1992); Phys. Rev. Lett. **69**, 737 (1992).
- [32] S. Alamoudi *et al.*, Phys. Rev. D **60**, 125003 (1999).
- [33] J. Randrup, Phys. Lett. **92**, 122301 (2004).
- [34] W. N. Zhang, Y. M. Liu, L. Huo, Y. Z. Jiang, D. Keane, and S. Y. Fung, Phys. Rev. C **51**, 922 (1995).
- [35] W. N. Zhang, G. X. Tang, X. J. Chen, L. Huo, Y. M. Liu, and S. Zhang, Phys. Rev. C **62**, 044903 (2000).
- [36] C. Y. Wong and W. N. Zhang, Phys. Rev. C **70**, 064904 (2005).
- [37] W. N. Zhang, S. X. Li, C. Y. Wong, and M. J. Efaaf, Phys. Rev. C **71**, 064908 (2005).
- [38] W. N. Zhang and C. Y. Wong, IJMPE **16**, 3262 (2007); C. Y. Wong and W. N. Zhang, IJMPE **16**, 3271 (2007).
- [39] M. Gyulassy, D. H. Rischke, and B. Zhang, Nucl. Phys. **A613**, 397 (1997).
- [40] H. J. Drescher, F. M. Liu, S. Ostapchenko, T. Pierog, and K. Werner, Phys. Rev. C **65**, 054902 (2002).
- [41] Y. Hama, T. Kodama, and O. Socolowski Jr, hep-ph/0407264.
- [42] R. P. G. Andrade, F. Grassi, Y. Mama, T. Kodama, and W. L. Qian, Phys. Rev. Lett. **101**, 112301 (2008).
- [43] Yan-Yu Ren, Wei-Ning Zhang, Jian-Li Liu, Phys. Lett. B **669**, 317 (2008).
- [44] D. A. Brown, R. Soltz, and A. Kisiel, Phys. Rev. C **76**, 044906 (2007).
- [45] S. Pratt, T. Csörgo, and J. Zimányi, Phys. Rev. C **42**, 2646 (1990).

- [46] S. E. Koonin, Phys. Lett. **70B**, 43 (1977).
- [47] Available on the CERN Program Library webpage,  
URL:<http://wwwasd.web.cern.ch/wwwasd/index.html>.
- [48] J. P. Blaizot and J. Y. Ollitrault, Phys. Rev. D **36**, 916 (1987).
- [49] E. Laermann, Nucl. Phys. **A610**, 1 (1996).
- [50] D. H. Rischke and M. Gyulassy, Nucl. Phys. **A608**, 479 (1996).